Formation of Linear and Graft Block Copolymers at a Polymer/Polymer Interface: How Copolymer Brush and Microdomain Morphology Control Heterogeneous Reactions

ARTICLE *in* MACROMOLECULES · NOVEMBER 2012

Impact Factor: 5.8 · DOI: 10.1021/ma301697n

3 AUTHORS:

Anatoly V Berezkin
Technische Universität München
30 PUBLICATIONS **173** CITATIONS
SEE PROFILE

Daria V Guseva
Lomonosov Moscow State University
8 PUBLICATIONS **42** CITATIONS
SEE PROFILE

Yaroslav V Kudryavtsev
Russian Academy of Sciences
62 PUBLICATIONS **355** CITATIONS
SEE PROFILE

Macromolecules

Article

pubs.acs.org/Macromolecules

Formation of Linear and Graft Block Copolymers at a Polymer/Polymer Interface: How Copolymer Brush and Microdomain Morphology Control Heterogeneous Reactions

Anatoly V. Berezkin,[†] Daria V. Guseva,[‡] and Yaroslav V. Kudryavtsev[§,*]

[†]Max-Planck Institut für Eisenforschung GmbH, Max-Planck Strasse 1, 40237 Düsseldorf, Germany

[‡]Physics Department, Lomonosov Moscow State University, Leninskie gory, 1, build. 2., 119991 Moscow, Russia

[§]Topchiev Institute of Petrochemical Synthesis, Russian Academy of Sciences, Leninsky prosp. 29, 119991 Moscow, Russia

ABSTRACT: Irreversible coupling between immiscible melts of two functionalized macromonomers A and B of different lengths resulting in the formation of a linear or graft block copolymer AB was modeled by dissipative particle dynamics. Recently (*Macromolecules* **2011**, *44*, 112), we investigated the mechanism of the instability caused by saturating an A/B interface with the copolymer product, which leads to a microdomain structure formation. The present simulations were focused on the influence of copolymer composition and architecture on the microstructure development and characteristics of different kinetic regimes. Nearly symmetric copolymers form bicontinuous microdomains facilitating mass transfer and resulting in the exponential coupling kinetics. Strongly asymmetric copolymers promote fragmentation of a minor phase into isolated domains hardly accessible for the remaining reactants so that the linear or even slower kinetics is observed. At an equal concentration of functional groups, grafting proceeds always slower than end-coupling since branched copolymers form less penetrable brushes at the interface than linear diblocks. The most effective screening is achieved with symmetric copolymers. Both end-coupling and grafting produce long-lived nonuniform microstructures, with the size and shape of domains monotonously changing along the distance from the initial A/B interface. In the interface vicinity, minor phase micelles can form ordered layers.

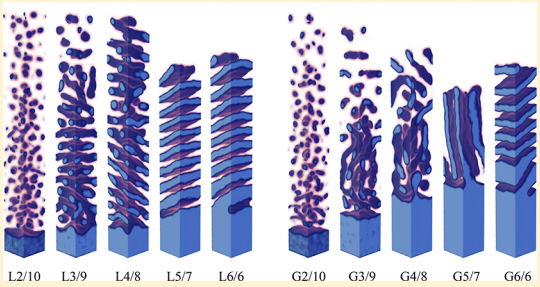

INTRODUCTION

Industrially, the most efficient way to design plastics with desired properties is mixing a few widely produced polymers, as alternative to more complex and expensive synthesis of new high-molecular compounds.[1] However, such blending is not a simple task since most of the polymer pairs are thermodynamically incompatible. Even upon coextrusion of polymer melts, microscopy reveals micrometer-size inhomogeneities that lead to a relatively small interfacial area and weak adhesion between blend components resulting in poor mechanical properties of a composite.[2] The straightforward way to enhance miscibility is adding a premade copolymer compatibilizer but, aside from preparation costs, it often encounters a delivery problem when the additive forms idle micelles within bulk phases instead of diffusing to a polymer/polymer interface.[3] A promising alternative strategy is the reactive compatibilization,[1,4−7] which implies *in situ* copolymer formation directly during blending of homopolymer melts. Though preparing functionalized macromolecules is required, it is very advantageous that copolymer chains appear at the interface just where they are needed.

Whereas the reactive compatibilization has gained practical success in polymer engineering,[8] understanding its mechanism on the molecular level is still lacking due to heterogeneous nature of reactions involving long-chain reactants. Various factors (diffusion, reaction, accumulation of the reaction products, phase structure, force mixing) can be separated and described only for relatively simple model systems. One of the most popular models is a flat interface between quiescent melts of two incompatible homopolymers bearing complementary reactive groups at the chain ends or along their backbones. An irreversible coupling reaction produces linear or graft block copolymers, which remain at the interface improving adhesion, fracture toughness, etc.[9−11] and, in turn, influence the reaction kinetics. Such a model system was extensively investigated in theory,[12−18] by simulations,[19−25] and by experiment.[18,26−38]

Theoretical studies revealed how the reaction between chain ends proceeds at a nearly free interface and how it slows down due to the formation of a copolymer brush and/or reactant depletion in the interfacial layer. At the earliest stage of a bimolecular reaction, the interfacial coverage n (the number of copolymer chains per unit area of the initial interface) grows linearly with time t

$$n(t) \sim t\rho_A\rho_B \quad (1)$$

Received: August 10, 2012
Revised: September 25, 2012
Published: October 17, 2012

   dx.doi.org/10.1021/ma301697n | *Macromolecules* 2012, 45, 8910−8920

where ρ_A, ρ_B are the bulk densities of reactive A and B groups, respectively. This very short linear stage (the reaction controlled regime) is hardly observed in laboratory experiments but can be well reproduced by simulations at low reactivities.[24]

As soon as copolymer chains saturate the interface, repulsion and stretching of their blocks become an important kinetic factor. This takes place at some critical coverage $n_{cr} = 1/(3N^{1/2}b^2)$, where b is a segment size. The copolymer brush creates a potential barrier for unreacted homopolymers, leading to the following logarithmic kinetics:[15]

$$n(t) \sim n_{cr}\sqrt{\ln\left(\frac{N^{1/2}t}{\tau \ln N}\right)} \tag{2}$$

where τ is the terminal chain relaxation time. Such dependence (the saturation regime) is reproduced by simulations[19,23−25] at moderate reaction rates and $\rho_A \approx \rho_B$ being established after the linear regime (eq 1).

Experiments demonstrated that, under all practical conditions, the coupling is controlled by the reactivity of functional groups.[26] In some cases, namely for relatively low-molecular masses and high functionalization degrees of the initial homopolymers, the reaction did not cease and even got faster in parallel to a considerable increase in the interface roughness and/or blend viscosity.[18] Similar effects promoting emulsification were reported for the blends that react under mixing conditions.[39−41] It was supposed[35,40] that an in situ formed copolymeric surfactant lowers interfacial tension thus making the interface less stable, yet such concept does not explain the molecular mechanism of interfacial roughness development. Moreover, the heterogeneous kinetics is still not much explored because finding the amount of formed copolymer at a given time involves complicated scattering spectrometry or chromatography techniques.

The instability was reproduced in computer simulations,[19,23] but only recently was it explicitly demonstrated[24] that it occurs when the interfacial copolymer coverage n exceeds a saturation value n_s, which is close to the equilibrium coverage for a phase-separated melt of the pure copolymer product. Thus, the interfacial roughening is triggered by steric forces between adsorbed copolymer chains that are also known to be responsible for stabilizing a droplet phase in blends against coalescence.[42−44] The instability takes place prior to a substantial decrease in the interfacial tension[24] and therefore it is not governed by thermal fluctuations. Conversely, roughening is an irreversible, thermodynamically beneficial process, which proceeds only as long as the polymers react.

With simulations, different kinetic regimes of end-coupling at polymer/polymer interfaces were delineated[24] and the role of polydispersity was studied.[25] In particular, it was found that the instability development in a symmetric system is described by the exponential kinetics, when each new portion of the product creates more area for further reactions:

$$n(t) = n_s \exp\left(\frac{k_s \rho_A \rho_B}{n_s}(t - t_s)\right) \tag{3}$$

Here k_s is the rate constant, t_s is the characteristic time when roughening starts. Equation 3 perfectly describes the coupling kinetics at $t > t_s$ when an instability develops (the autocatalytic regime), but soon the exponential growth is replaced by a terminal, diffusion-controlled-like regime

$$n(t) \sim t^{1/2} \tag{4}$$

Asymptotic behavior of eq 4 is consistent with the experimental data on the coupling kinetics in PS/PMMA systems.[32,33] The reaction rate in the terminal regime is limited by diffusion through the mature microdomain structure formed by a copolymer product at the interface.

In this paper we extend the class of modeled systems to include irreversible grafting reactions and compositionally asymmetric polymer blends. Our study aims at finding answers to the following principal questions. (i) End-coupling kinetics in symmetric systems includes four regimes.[24] What general picture will be observed if the blend components have different chain lengths and if the reaction is grafting? (ii) Copolymer product at the interface forms a brush that impedes further reactions. How effective is the brush depending on its topology and degree of asymmetry? (iii) Interfacial instability in a lamella-forming cocontinuous blend leads to a very fast, exponential kinetics. What will happen in an asymmetric system with only one continuous phase? Besides, we would like to check our previous finding[24,25] that the interfacial instability preceding the microstructure formation can be attributed to attaining the copolymer interfacial density peculiar to a corresponding fully reacted microphase separated system.

It is worth mentioning that grafting, which requires end-functionalization of only one component, is used for practical compatibilization of immiscible polymers for decades.[1,4,9−11,28−31,40,41,45,46] Naturally, the instability was first reported for an interface filled with *in situ* formed graft block copolymers,[47] which are believed to be more effective in reactive compatibilization than corresponding linear diblocks.[29,48,49] A systematic comparison of the end-coupling and grafting kinetics for the same functional groups attached to polymers in solutions, homo- and heterogeneous melts[30] demonstrated that an effective rate constant is always higher for the reaction between end groups, the difference being most pronounced (of the order of 10) for a static bilayer system. At the same time, theoretical investigations or simulations of interfacial grafting are scarce[12,18,22] and do not reveal peculiarities of that important type of macromolecular reactions, thus motivating the present study.

MODEL AND SIMULATION TECHNIQUE

We use a mesoscopic molecular dynamics technique referred to as dissipative particle dynamics (DPD), which was proposed by Hoogerbrugge and Koelman[50,51] and developed by Espanol, Groot, and Warren.[52,53] Polymer chains are modeled as soft particles (units) connected by harmonic springs. Detailed description of the model and a brief review of applying DPD to polymer systems can be found in our previous papers.[24,25] We take the average density of particles $\rho_0 = 3$, noise amplitude of the random force $\sigma = 3.0$, and amplitude of the conservative repulsive force between similar particles $a_{ii} = 25$. The repulsion parameter for dissimilar particles a_{ij} is related to the interaction parameter χ of the Flory−Huggins theory as[53]

$$a_{ij} = \chi_{ij}/0.306 + 25 \tag{5}$$

In our simulations of immiscible melts A and B, the typical value is $a_{AB} = 50$, so that if a diblock copolymer of $N \sim 10$ monomer units is formed, it enters the strong segregation regime[54] with $\chi N \sim 10^2$, when blocks are rather incompatible and the copolymer is accumulated at the A/B interface.

dx.doi.org/10.1021/ma301697n | Macromolecules 2012, 45, 8910−8920

The equations of particle motion were solved using the so-called DPD−VV integration scheme[55] (modified velocity−Verlet algorithm) with the time step $\delta t = 0.04$.

Chemical reactions were modeled using a probabilistic approach based on the following principles.[24]

1 Two functionalized particles can react (form a new bond) at a short distance only, which is called the reaction radius r_R (here $r_R = 1$ as well as the cutoff radius for all DPD forces).
2 Each pair of contacting functionalized particles is considered for the possible reaction in a random order.
3 Reaction in every pair proceeds with a certain predefined probability p_0 at moments separated by equal time intervals Δt (every 10th step in our simulations so that $\Delta t = 10\delta t = 0.4$).
4 If the average number of pairs simultaneously formed by a functionalized particle equals η, then the product ηp_0 gives the probability of particle consumption at a given reaction step. Since an active particle can react only once, p_0 value should obey the inequality $\eta p_0 < 1$. Otherwise, the reaction rate will be underestimated because the number of reacted particles will be lower than expected from given values of p_0 and concentration.

The reaction probability per unit time, $p_R = p_0/\Delta t$, was varied from 0.0025 to 0.25 but most of the results discussed below correspond to $p_R = 0.025$, when an appropriate balance between the simulation time and experimentally realistic reaction controlled kinetics is attained. An estimate of the relation between DPD time and real time can be found in ref 24.

Similar approaches were implemented in previous MD,[56,57] DPD,[58,59] and Monte Carlo[60] simulations of polymerization and polycondensation.

Simulation box initially contained two layers of immiscible macromonomers A and B separated by a nearly flat interface parallel to the *xy* plane as illustrated in Figure 1. Each chain B possessed one reactive end group while chains A could be end-functionalized (Figure 1a) or multifunctionalized (Figure 1b), with first reactive group at one of its ends and other groups evenly distributed along the backbone. An irreversible coupling, which was possible only between dissimilar macromonomers, led to the formation of linear or graft copolymer AB, respectively.

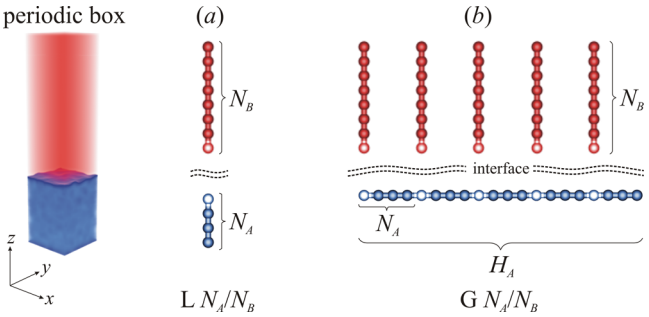

Figure 1. Structure of the initial systems (a) L4/8 ($N_A = 4$, $N_B = 8$) and (b) G4/8 ($N_A = 4$, $H_A = 20$, $N_B = 8$) for simulating irreversible end-coupling and grafting reactions at a polymer/polymer interface. Reactive units A and B containing complementary functional groups are highlighted.

In order to elucidate the role of copolymer composition and topology, the numbers of A and B units per one reactive unit of the corresponding type, N_A and N_B, were varied, while their sum $N = N_A + N_B = 12$ and the polymerization degree of a chain A, $H_A = 18-20$, were kept constant. Test simulations of grafting macromonomers B onto longer chains A with $H_A = 36-40$ and the same structure of repeating copolymer fragment demonstrated almost the same kinetics in all regimes.

Designations of the considered systems, L2/10, L3/9, L4/8, L5/7, and L6/6, as well as G2/10, G3/9, G4/8, G5/7, and G6/6 are clear from Figure 1, where a letter defines the copolymer type (L, linear; G, graft) and the slash-separated numbers are N_A and N_B. Note that $H_A = 18$ for G3/9 and G6/6, whereas $H_A = 20$ for G2/10, G4/8, and G5/7 systems.

The overall blend composition depended on the ratio N_A/N_B to keep equal numbers of the complementary functional groups. It means that the systems L2/10 and G2/10 were the most asymmetric with respect to both the blend composition and that of the copolymer product.

Impenetrable walls made of particles similar to the particles of an adjacent melt were used in the *z* direction and the periodic boundary conditions were imposed in the *x* and *y* directions. Massive simulations demonstrated that a minimal box cross-section for which the kinetics is not influenced by the periodic boundary conditions is $l_x = l_y = 20$. Thus, simulation boxes of sizes $l_x \times l_y \times l_z = 20 \times 20 \times 80$ (96000 particles) and $l_x \times l_y \times l_z = 20 \times 20 \times 300$ (360000 particles) were used at mid- and long-term time scales, respectively. After an initial relaxation for 10^5 steps, the simulation time was up to 2×10^7 steps (8×10^5 dimensionless time units). All the results were averaged over eight independent runs.

RESULTS AND DISCUSSION

Initial Reactivity. The coupling kinetics at early stages can be influenced by (i) the nonhomogeneous distribution of reactive units across the initial interface and (ii) the dependence of the reactivity of functional groups on their positions in chains. In order to estimate those effects we modeled an equilibrium state in the same but nonreactive bilayer melts of immiscible homopolymers A and B. After relaxation for 10^5 steps and averaging over subsequent $10^5\delta t = 4 \times 10^3$ time interval, the density profiles of A and B units, ρ_A and ρ_B, and the density of contacts between A and B end groups at the interface, ρ_{AeBe}, were calculated and plotted in Figure 2.

The left plot (Figure 2a) compares the scaled densities $\rho_A(z)/N_A$ and $\rho_B(z)/N_B$ with those of corresponding end groups $\rho_{Ae}(z)/2$ and $\rho_{Be}(z)/2$, respectively. It is seen that the reaction zone, where complementary functional groups can meet, is noticeably shifted for asymmetric systems to the side occupied by a longer macromonomer. In the case L2/10 ($N_A = 2$) $\rho_A(z) \equiv \rho_{Ae}(z)$ by definition, but for longer A macromonomers the difference between these profiles becomes visible. It can be explained by enrichment of the interface with chain ends, which is well-known from both the theory[61,62] and experiment.[63] The same effect is revealed in Figure 2b, where the interfacial density of AB end contacts (two particles are in contact if their centers are separated by less than the unit distance), ρ_{AeBe}, grows if N_B is increased at a constant N_A. Note that the value of ρ_{AeBe} can be used as a measure of the initial reactivity for a system with functional groups. Among our L models, for which $N_A + N_B$ is fixed, it attains a maximum for the

dx.doi.org/10.1021/ma301697n | *Macromolecules* 2012, 45, 8910−8920

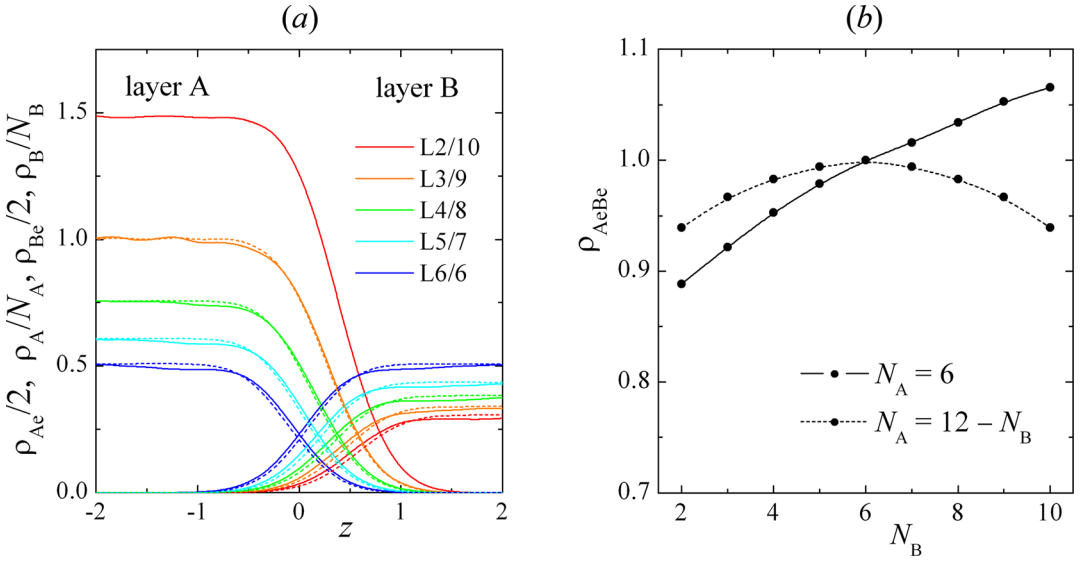

Figure 2. (a) Scaled density profiles of A and B end groups, $\rho_{Ae}/2$ and $\rho_{Be}/2$, (solid lines) and of A and B units, ρ_A/N_A and ρ_B/N_B, (dashed lines) across the initial interface in LN_A/N_B systems. (b) Reduced density of contacts between A and B end groups, ρ_{AeBe}, for different lengths of macromonomers B at fixed $N_A = 6$ (solid line) or fixed $N_A + N_B = 12$ (dashed line). The reference system with $\rho_{AeBe} = 1.0$ is L6/6.

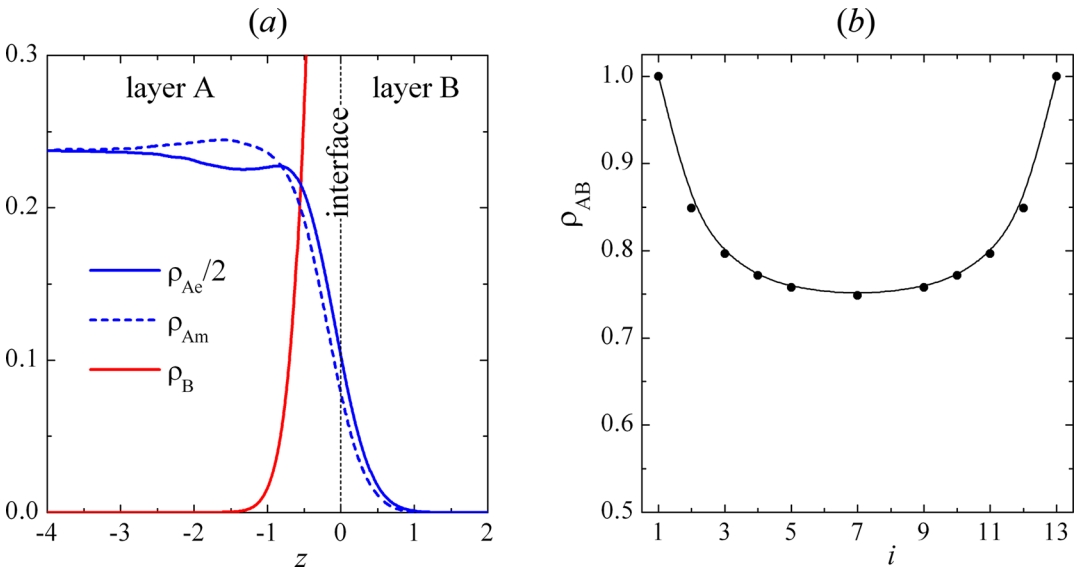

Figure 3. (a) Density profiles of end and middle A units, $\rho_{Ae}/2$ and ρ_{Am}, and all B units, ρ_B, across the initial interface. (b) Reduced density of AB contacts, ρ_{AB}, depending on the position of an A unit in its chain. Macromonomer lengths are $N_A = 13$ and $N_B = 6$.

symmetric melt L6/6, however, the drop for other modeled systems does not exceed 6%.

It is worth recalling that, contrary to heterogeneous reactions considered in this study, the effective reactivity of end groups in a homogeneous melt slightly decreases with the macromonomer length[24] due to the partial screening of functional groups by their chain neighbors.

For macromonomers consisting of more than ten units, growing segregation of end groups to the interface results in the appearance of a minimum at the end group density profile $\rho_{Ae}(z)$ (Figure 3a), in agreement with the theoretical analysis for long chains.[61,62] Enrichment of the interfacial area with end groups is clearly seen from Figure 3b, where the reduced density of AB contacts ρ_{AB} is plotted depending on the position of an A unit in its chain. As a result, end-coupling at a nearly free interface should proceed faster than grafting under the same conditions, as was found in the laboratory experiments.[30] The reactivity ratio of ~10 reported in ref 30 is much higher than 1.7 that follows from Figure 3b, but the experimental value was found using the kinetic curve, whereas we estimated the initial reactivities. As mentioned in ref 30, higher interfacial mobility of terminal units than middle ones[64] can also increase the rate of end-coupling in comparison to grafting.

General Trends in the Kinetics. Time dependencies of the interfacial copolymer coverage assuming a flat interface, n, are plotted in Figure 4 for the reactions yielding asymmetric linear or graft block copolymers. The curves at least qualitatively reproduce the sequence of four regimes mentioned in the Introduction. It is seen that the copolymer composition and topology noticeably influence the kinetics from the instability outset onward. The kinetics in the regime III is faster than in the previous one but exponential only for some of the studied systems. Therefore, it is more convenient to use the term "acceleration regime" instead of "autocatalytic regime" in

dx.doi.org/10.1021/ma301697n | Macromolecules 2012, 45, 8910−8920

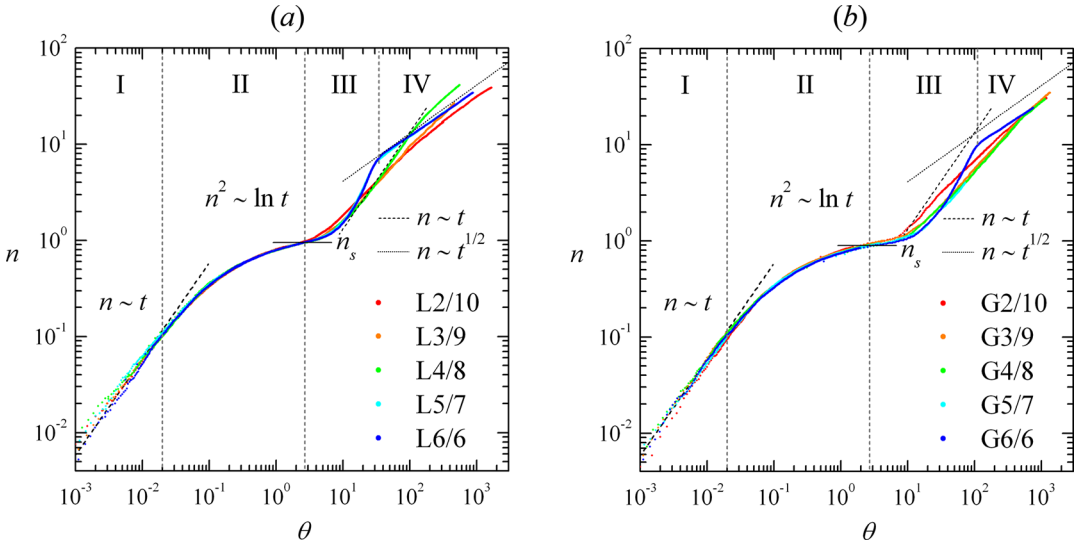

Figure 4. Full kinetic curves for (a) end-coupling and (b) grafting reactions in different model systems. The dependences of the interfacial copolymer coverage n on the scaled time θ (defined in eq 7) are plotted for p_R = 0.025 and a_{AB} = 50. Reaction-controlled (I), saturation (II), acceleration (III), and terminal (IV) regimes are separated by vertical gray lines (plotted for the systems L6/6 and G6/6). The saturation coverage n_s and theoretical trends $n \sim t$ and $n \sim t^{1/2}$ are shown.

refs 24 and 25. Earlier, in the saturation regime, the effect of copolymer composition is observed only in the case of grafting. At the earliest stage conversion fluctuations around the common linear trend are visible. Below we discuss the reaction in each regime in more detail.

Reaction Controlled Regime. If the copolymer coverage and depletion of reactants are negligible, the initial kinetics of irreversible end-coupling at a polymer/polymer interface approximately obeys the second-order mean field law[13,14]

$$\frac{dn}{dt} \approx k_0 \rho_A^0 \rho_B^0 = \frac{k_0 \rho_0^2}{N_A N_B} \qquad (6)$$

where k_0 is the reaction rate constant ($k_0 \sim p_R$), ρ_A^0 and ρ_B^0 are the initial bulk densities of reactive units. Since there is nothing special about the reaction mechanism in eq 6, we can apply it to grafting as well, with a more general definition of n as the number of newly formed A-B bonds per unit area of the xy face of the simulation box.

Integration of eq 6 yields a linear time dependence of n similar to eq 1:

$$n = K\theta, \quad K = \text{const}, \quad \theta = \frac{t p_R}{N_A N_B} \qquad (7)$$

This regime is well reproduced in our simulations for both end-coupling and grafting reactions (Figure 5).

Equation 7 satisfactorily approximates the kinetic curves for all systems corroborating that the process is reaction controlled. Variations due to the different macromonomer lengths and positions of reactive groups, which we discussed above for the initial systems, cannot be discriminated from concentration fluctuations, which are rather high at the very fast initial stage. Nevertheless, we will see that the asymmetry and topology factors play an important role at the subsequent stages of the process.

Saturation Regime. It is seen from Figure 5 that the regime I is over at $\theta \approx 0.02$. In accordance with the theoretical analysis by O'Shaughnessy and Vavylonis,[16] for our model characterized by low reactivity and complete functionalization

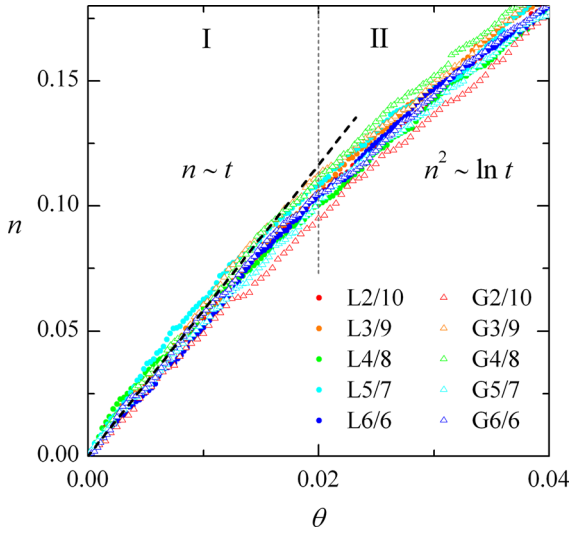

Figure 5. Initial kinetics of end-coupling and grafting in the reaction controlled regime I. The black dashed line represents the linear trend.

of macromonomers, the linear growth of conversion is followed by saturation. The reaction rate is slowed down due to the formation of a copolymer brush that thickens with time thus making a potential barrier for reactants higher. Since eq 2 predicting the logarithmic kinetics was derived in ref 16 for end-coupling of two polymers of equal length, it was interesting to check whether it holds for other model systems. Simulations demonstrated (Figure 6a) that the block length ratio does not influence the kinetics of end-coupling in L systems at a fixed copolymer chain length $N = N_A + N_B$. On the contrary, systems undergoing grafting exhibited noticeable retardation, which was dependent on N_A/N_B and most pronounced for the symmetric melt G6/6, though the kinetics remained logarithmic.

It is not surprising that a copolymer brush with branched architecture slows down the interfacial reaction more effectively than a brush containing linear chains. The theoretical analysis revealed[65] that a brush formed by graft copolymers is thinner and chains are more stretched because, using adsorption

dx.doi.org/10.1021/ma301697n | Macromolecules 2012, 45, 8910−8920

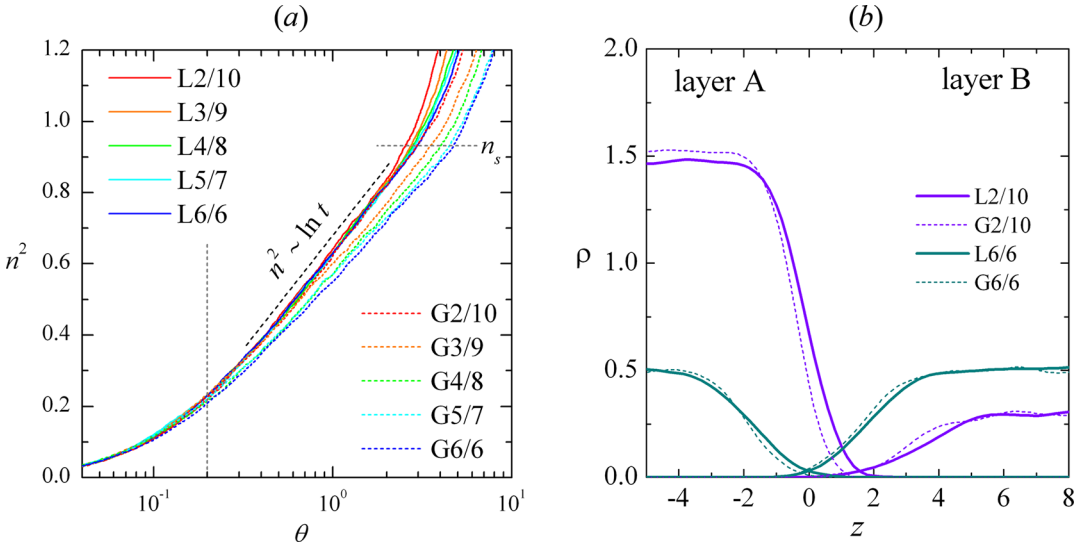

Figure 6. (a) Saturation regime of end-coupling and (b) density of A and B reactive units across the initial interface at the end of the saturation regime (n = 0.9 for all the systems). Gray dashed lines mark the beginning and end of the regime II, black dashed line shows the logarithmic fit according to eq 3.

terminology, loops are formed instead of tails. Having plotted in Figure 6b the interfacial profiles of reactive units for two symmetric (L6/6, G6/6) and two asymmetric (L2/10, G2/10) systems, we found that the brushes in G systems are indeed more "dry"; i.e., unreacted macromonomers are expelled from the reaction zone. Among different G systems, the most pronounced effect was observed for the G6/6 melt that demonstrated the slowest kinetics.

However, it was not clear why the asymmetric systems L2/10 and G2/10 exhibit notably deviating distributions of reagents (Figure 6b) but very small difference in the reaction rate (Figure 6a)? We supposed that a multifunctionalized macromonomer A undergone first grafting gets anchored at the interface so that other functional groups of the same chain have more chances to react (see the scheme in Figure 7). Such effect

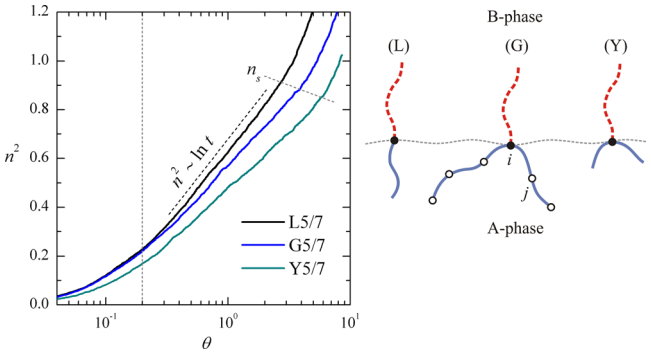

Figure 7. Comparison of the kinetics in the saturation regime II for the systems L5/7, G5/7, and Y5/7, in which linear, graft, and Y-shaped copolymers are formed. Grafting of a B end to any A unit anchors other functional A groups of the same chain to the interface.

was considered by one of us in theory[66] and it was found that if an ith monomer unit of a polymer chain is anchored at some surface, the probability of a contact between jth unit of the same chain and the surface is proportional to $1/|i - j|$. Therefore, anchoring should accelerate the kinetics in our models and the most pronounced effect is expected when reactive A units are situated most closely to each other along the backbone, which takes place in the G2/10 system. In more symmetric G systems (Figure 6a), the reaction is slowed down due to both thickening of an A side of the brush and weakening of the anchoring effect.

In order to check this assumption, we carried out additional simulations. Long A chains of the length H_A were divided into short fragments of length N_A each containing one functional group attached to a middle unit. Grafting in such model system leads to Y-shaped copolymers, but without any anchoring effect. Comparing the simulation results for L5/7, G5/7, and Y5/7 systems shown in Figure 7, we see that the system with Y-shaped copolymers exhibits the slowest kinetics. We may conclude that the copolymer architecture plays an important role in the saturation regime II, however, this is partially compensated by the anchoring effect, which in turn depends on the density of functionalized groups in polymer chains. If not all chains are functionalized, it is very likely that the effect of anchoring can even override that of the brush architecture resulting in a faster kinetics for grafting in comparison to end-coupling.

Interfacial Instability. As was demonstrated in our simulations of end-coupling in symmetric systems,[24,25] a copolymer brush can considerably suppress interfacial reactions, which are however not ceased and new portions of the product are formed at the interface. At a certain time t_s (though it can be practically inaccessible for long chains[32]) the interface becomes saturated and unstable so that further couplings result in a dramatic growth of the interfacial area through roughening. The reaction in turn gets accelerated and this is marked by an upward inflection point on the kinetic curve. Such points designating the boundary between the saturation regime II and acceleration regime III for different model systems are clearly seen in Figures 4 and 6a.

It was found[24] that the saturation coverage $n_s = n(t_s)$ divided by the dimensionless area of the initial interface S_0 is close to the equilibrium interfacial density of chains, c_∞, in the melt of a diblock copolymer, which is formed in the reacting system at 100% conversion:

$$c_\infty \approx n_s/S_0 \qquad (8)$$

dx.doi.org/10.1021/ma301697n | Macromolecules 2012, 45, 8910−8920

In the present study, we checked whether eq 8 holds for asymmetric and grafted systems. Instead of modeling the coupling up to its end, we used the DPD technique to simulate microphase separation in the premade diblock copolymer melts at a_{AB} = 50. The interface area S_0 was calculated using the triangulation procedure as described in ref 24. The results summarized in Figure 8 corroborate the validity of eq 8 except

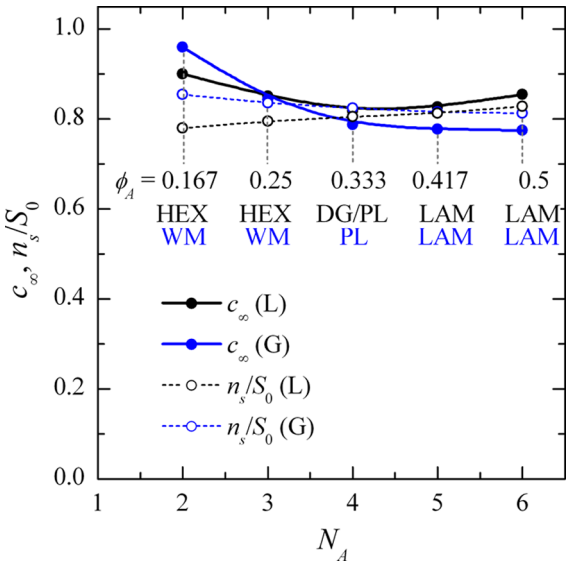

Figure 8. Interfacial density of copolymers chains at the end of the saturation regime in L and G systems, n_s/S_0 (dashed lines), and at the equilibrium state in the corresponding AB linear and graft block copolymer melts, c_∞ (solid lines). ϕ_A is the volume fraction of A units. Black and blue letters designate microstructures predicted in the literature[67,68] for linear diblocks and found in the present study for graft ones: hexagonally packed cylinders (HEX), double-gyroid phase (DG), perforated lamellas (PL), lamellas (LAM), and worm-like micelles (WM).

for the most asymmetric systems and thus confirm the idea that the interfacial instability develops similar to a phase separation process. It is also seen from Figure 8 that c_∞ only weakly depends on the blend composition, copolymer architecture, and, therefore, type of the equilibrium microstructure. Such conclusion is in agreement with Figure 6, where acceleration in the kinetics occurs at nearly the same saturation coverage n_s for all considered model systems (though G systems, in which slowing down the reaction is more pronounced, exhibit the instability later on the time scale than corresponding L systems).

Difference in the types of equilibrium structures for premade linear and graft copolymers can be understood having in mind the so-called constituting block copolymer hypothesis,[69] which says that the phase behavior of graft copolymers is similar to that of imaginary Y-shaped block copolymers obtained by cutting chain backbones in the middle between each pair of neighbor grafting points. Basing on that approach, theoretical analysis[65] and DPD simulations[70] demonstrated that the phase diagram of graft copolymers is substantially shifted in comparison to that of linear diblocks, whereas a complex topology often impedes ordering into long-range microdomain structures. In our case, worm-like micelles and perforated lamellas were observed in the melts of asymmetric graft copolymers instead of the hexagonal structure and double-gyroid in the corresponding melts of linear diblocks. A complete investigation of the microstructures should also include the analysis of system size effects, which was not involved in this study.

Late Stages. Turning back to the L and G models, let us consider how a microdomain morphology develops in reacting melts. Figure 9 demonstrates the scenario for the strongly

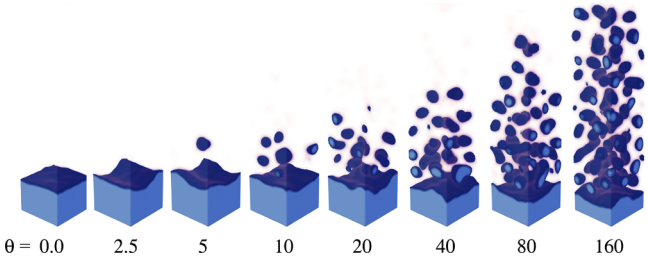

Figure 9. Evolution of the system L2/10. The simulation box size is 20 × 20 × 80. Only A phase is shown.

asymmetric system L2/10. Contrary to the symmetric lamella-forming blend (see Figure 3 of ref 24), the AB copolymer is organized into micelles that all populate the major B phase, while the initial A/B interface moves with the shrinking A layer. New micelles are regularly emitted from the interface, which preserves high roughness attained at saturation. Morphological deviations from the melt of a copolymer product are related to the presence of unreacted macromonomers within microdomains. For example, the microstructure of L2/10 shown in Figure 9 is dominated by disordered micelles, while in the corresponding copolymer melt hexagonally packed cylinders are expected, as follows from Figure 8.

Looking at the structures formed by various model systems, which are shown in Figure 10, one finds that at a fixed N_A/N_B

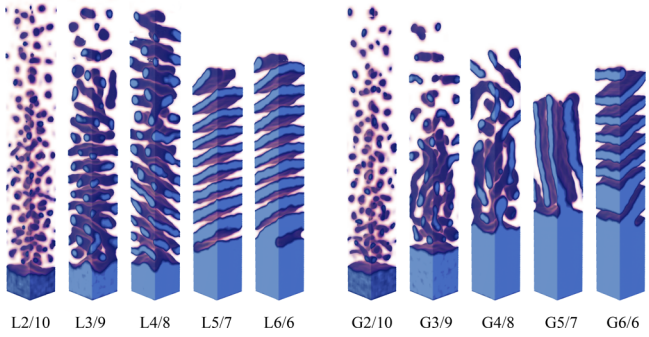

Figure 10. Reacting L and G systems of different compositions after 10^7 integration steps (θ = 500, 370, 312, 286, and 278 for N_A = 2, 3, 4, 5, and 6, respectively). The simulation box size is 20 × 20 × 160. Only the A phase is shown.

ratio G and L systems exhibit similar (in shape, size, and connectivity of domains) local morphologies, though their degrees of macroscopic ordering can be considerably different. Then, it is worth noting that the microstructure characteristics depend not only on the copolymer and blend composition but also vary in the z (vertical) direction. Such effect can be explained by a nonhomogeneous distribution of species, which is close to the equilibrium copolymer ratio near the initial interface but shifted to the excess of B units as one moves up in the z direction. By varying blend asymmetry one can change characteristics and even type of the local microstructure. For

dx.doi.org/10.1021/ma301697n | Macromolecules 2012, 45, 8910−8920

instance, in the systems L2/10 and G2/10 cylinders are observed near the remaining A layer and spherical micelles in the rest part of the melt. In the systems L3/9 and G3/9, one can see a gradual transition from uniaxially ordered cylinders to short disordered cylinders and then to spheres. In the system L4/8, perforated lamellas transform into cylinders, whereas in the corresponding pure copolymer melt usual lamellas are observed. The systems L5/7, L6/6, and G6/6 exhibit lamellas of varying thickness, which decreases with the distance from the parent layer. Gradient effects in the melt morphology are mostly noticeable at the end of the acceleration regime III.

It should be pointed out that all nonuniform structures depicted in Figure 10 are thermodynamically nonequilibrium, though long-living, ones. Their relaxation time is comparable with the duration of the acceleration regime. Orientation of highly ordered structures like parallel lamellas or cylinders is affected by limited sizes of the model systems. In laboratory conditions, long-range ordering can be suppressed by stochastic convective flows even without force mixing. Experiments demonstrate[40] that the orientation of domains is more or less arbitrary, being governed by large-scale hydrodynamic fluctuations, which cannot be reproduced in a small model system.

Below we discuss how morphology governs the late stage kinetics in the L and G systems, which is plotted on the large scale in Figure 11. Considering the dependence of the

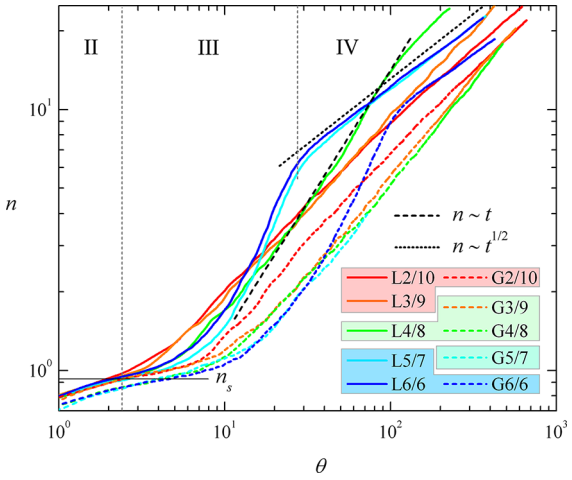

Figure 11. Interfacial copolymer coverage n plotted vs scaled time θ for the late stages (acceleration regime III and terminal regime IV) of end-coupling and grafting. Details are as in Figure 4. Systems with similar kinetics are colored together in the legend.

copolymer coverage n on time, it is possible to divide all systems into several groups: (L5/7, L6/6, G6/6), (L4/8, G3/9, G4/8), and (L2/9, L3/9, G2/10). The kinetic curve for G5/7 belongs to the first group in the regime III and to the second one in the regime IV reflecting the appearance of a lamellar structure, which later transforms into cylindrical micelles.

In the systems belonging to the first group, a lamellar structure is formed after roughening and their kinetics obeys the exponential law given by eq 4, which implies that any point of the interface is accessible for reactive chains via interconnected channels existing in bicontinuous phases (slanted lamellas in the simulation box are connected because of the periodic boundary conditions).

In nonlamellar systems the kinetics is much slower (note that Figure 11 is plotted on a double logarithmic scale). In the second group, it is nearly linear in time, similarly to eq 2, because the interfacial area attains some constant value after short growth caused by roughening. Systems of the third group that contain only one continuous phase demonstrate even slower kinetics. In that group, kinetic fluctuations are most pronounced, which is related to structural rearrangements in the ensemble of micelles.

Difference in the scenarios of reactive compatibilization in the symmetric and asymmetric systems is illustrated by Figure 12. This figure shows how the densities of A units and, specifically, reactive A units, calculated at a given distance from the initial interface, are changed in time. Interfacial instability in the symmetric system L6/6 (Figure 12a,b) launches the continuous process of lamella formation, which quickly destroys the bulk phases A and B and carries away reactive A units deeply into the opposite side of the simulation box. As lamellas are normally not perpendicular to the z axis, averaging in the xy plane makes the long-range order invisible in the density plot.

On the contrary, micelle formation in the asymmetric system L2/10 (Figure 12c,d) does not lead to the fast exhaustion of the bulk phases because reactive A units have no chance to leave their phase without encapsulation into a rather small micelle, where they rapidly react. Micelles diffusing deeply into the B layer do not contain reactive A units and their interfaces do not influence the effective reaction rate thus making eq 4 inapplicable. Such behavior is typical for all asymmetric nonlamellar systems.

Density waves are visible in Figure 12c, which means that micelles in the L2/10 system are ordered in the direction normal to the A/B interface. Though micelles are highly polydisperse in shape and size (Figures 9 and 10), the microstructure includes at least several layers and survives after averaging over eight independent runs so that its geometrical characteristics are well-defined. In the individual simulations, the ordering of micelles is even more pronounced. Orientation and stability of this liquid-like order are maintained by the interface, which repels the coronas of micelles in the first layer.

Microdomains that are continuously formed at the unstable A/B interface contain unreacted macromonomers, which are gradually consumed with time. Therefore, an instant concentration of the reactive species is nonuniform in the z direction with a gradient extending throughout the region occupied by the copolymer product. As a result, the kinetics becomes diffusion controlled and model systems enter the terminal regime IV, though not simultaneously. By modeling the systems L6/6 and L5/7 in the boxes with l_z = 80 and 300, it was shown that the characteristic time of entering the terminal regime does not depend on the system size so that the diffusion controlled kinetics is established due to the copolymer layer formation and not because of the reactant exhaustion in a simulation box.

It is seen from Figures 4 and 11 that most of the kinetic curves approach the diffusion controlled trend $n \sim t^{1/2}$. The crossover width drastically depends on the microdomain morphology. Indeed, the transition to the diffusion controlled regime is sharp for the lamellar systems L5/7, L6/6, G6/6 and extended in highly asymmetric micellar systems L2/10, G2/10. One can assume that all intermediate model systems between those limiting cases would be also governed by diffusion on a longer time scale. The diffusion control over late stages of the reactive compatibilization in quiescent polymer melts is corroborated[24] by the experimental data for PS/PMMA

dx.doi.org/10.1021/ma301697n | Macromolecules 2012, 45, 8910−8920

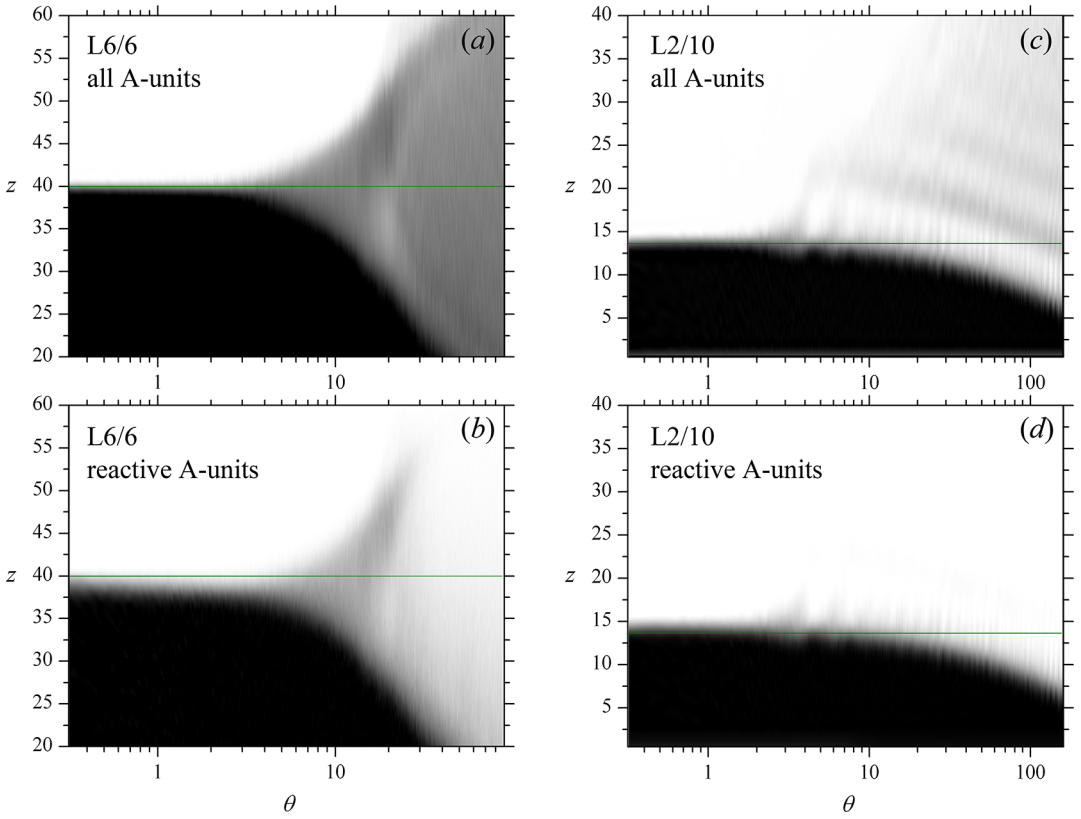

Figure 12. Grayscale average density of all A units (*a*,*c*) and reactive A units (*b*,*d*) in the systems L6/6 (*a*,*b*) and L2/10 (*c*,*d*) vs the coordinate z and scaled time θ. The green line marks an initial position of the A/B interface.

couple[32,33] obtained for $\chi(N_A + N_B)$ values comparable to those used in our study.

■ CONCLUSIONS AND OUTLOOK

In this study, the DPD modeling technique was used to simulate *in situ* formation of symmetric and asymmetric linear and graft AB block copolymers at the initially flat interface between two immiscible melts of functionalized homopolymers A and B. Now it is possible to answer the questions formulated in the Introduction.

(i) Generally, the kinetics of reactive compatibilization in an initially bilayer quiescent polymer melt includes four regimes: reaction controlled (the interface is nearly free), saturation (the copolymer product forms a brush-like interfacial layer), acceleration (the interfacial area grows giving more space to coupling reactions and copolymer layers are ordered into a microstructure), and terminal (the microstructure ripens and comes to the equilibrium, maybe through structural transformations). Within this general scenario, the copolymer composition and topology considerably influence the reaction kinetics.

(ii) Graft copolymers form less penetrable barrier at the interface then linear ones. Resulting gain in the retardation of coupling is partially compensated because once reacted multifunctionalized macromonomer stays at the interface and reacts again and again until a final graft copolymer is formed. Simulations demonstrate that, at a fixed $N_A + N_B$ value, the driest is the brush of a symmetric graft copolymer, in which case the slowest kinetics is observed.

(iii) Exponential kinetics is observed only in the blends with bicontinuous phases, where the interface is fully accessible for both reactants. In the strongly asymmetric systems, the instability leads to the formation of cylindrical or spherical micelles, which contain a limited number of reacting units. When they are consumed, such micelles do not any longer influence the reaction rate, which is thus determined mostly by the surface area of the remaining A layer. As a result, the linear or even slower kinetics is observed.

Also we found that the interfacial density of a nonreactive AB block copolymer, which corresponds to the coupling product in a reacting system and can be easily found by simulations, well approximates the saturation copolymer coverage n_s (an inflection point on the kinetic curve), which is attained at the moment when the flat initial interface becomes unstable. Thus, our previous result for the symmetric diblock copolymer melt[24,25] appears to be much more universal. The same is true for the diffusion control over the kinetics in the terminal regime though here we were not able to get the proof for all systems due to the computational limitations.

On our mind, two interesting observations of the present study deserve attention of experimentalists. First, we detected nonuniform morphologies in the course of the microstructure development in bilayer reacting polymer systems. The examples are coexisting cylinders and spheres or micelles of different width. They are formed according to the local blend and copolymer composition, which can vary in the direction perpendicular to the initial A/B interface, as a result of diffusion on a long time scale. Second, we demonstrated that the unstable A/B interface, as long as it is present in a reacting

system, organizes micelles, that are continuously emitted from it, into parallel layers.

Coarse-grained molecular dynamics simulations appeared very fruitful in the rather old area of reactive compatibilization. In the future, it seems very interesting to consider reactions at initially curved (say spherical) interfaces in order to visualize the evolution of a droplet or even a many-droplet system. *In situ* formation of a block copolymer can produce either stabilizing or destabilizing effects depending on the ratio of block lengths and particle size. Another opportunity to make use of molecular simulations is related to understanding flow effects in reacting polymer blends. A dramatic increase in the end-coupling reaction rate under elongational flow reported in ref 71 requires further investigation.

AUTHOR INFORMATION

Corresponding Author

*E-mail: yar@ips.ac.ru.

Notes

The authors declare no competing financial interest.

ACKNOWLEDGMENTS

The work was supported by the Russian Foundation for Basic Research (project 12-03-00817a). We thank A. A. Gavrilov for the parallel realization of the DPD code. We are also grateful for the opportunity to use computational cluster Chebyshev at the Moscow State University.

REFERENCES

(1) *Polymer Blends*; Paul, D. R., Bucknall, C. B., Ed.; Wiley: New York, 2000.
(2) Wool, R. P. *Polymer Interfaces: Structure and Strength*", Carl Hanser Verlag: New York, 1995.
(3) Anastasiadis, S. H. *Adv. Polym. Sci.* **2011**, *238*, 179.
(4) Koning, C.; Van Duin, M.; Pagnoulle, C.; Jerome, R. *Prog. Polym. Sci.* **1998**, *23*, 707.
(5) Litmanovich, A. D.; Platé, N. A.; Kudryavtsev, Y. V. *Prog. Polym. Sci.* **2002**, *27*, 915.
(6) Macosko, C. W.; Jeon, H. K.; Hoye, T. R. *Prog. Polym. Sci.* **2005**, *30*, 939.
(7) Jiang, G. J.; Wu, H.; Guo, S. Y. *Polym. Eng. Sci.* **2010**, *50*, 2273.
(8) Xanthos, M., Ed. *Reactive extrusion*; Hanser Publ.: Munich, Germany, 1992.
(9) Norton, L. J.; Smigolova, V.; Pralle, M. U.; Hubenko, A.; Dai, K. H.; Kramer, E. J.; Hahn, S.; Berglund, C.; DeKoven, B. *Macromolecules* **1995**, *28*, 1999.
(10) Tan, N. C. B.; Peiffer, D. G.; Briber, R. M. *Macromolecules* **1996**, *29*, 4969.
(11) Zhang, J.; Cole, P. J.; Nagpal, U.; Macosko, C. W.; Lodge, T. P. *J. Adhes.* **2006**, *82*, 887.
(12) Kramer, E. J. *Isr. J. Chem* **1995**, *35*, 49.
(13) Fredrickson, G. H. *Phys. Rev. Lett.* **1996**, *76*, 3440.
(14) O'Shaughnessy, B.; Sawhney, U. *Phys. Rev. Lett.* **1996**, *76*, 3444.
(15) Fredrickson, G. H.; Milner, S. T. *Macromolecules* **1996**, *29*, 7386.
(16) O'Shaughnessy, B.; Vavylonis, D. *Europhys. Lett.* **1999**, *45*, 638.
(17) O'Shaughnessy, B.; Vavylonis, D. *Eur. Phys. J. E.* **2000**, *1*, 159.
(18) Oyama, H. T.; Inoue, T. *Macromolecules* **2001**, *34*, 3331.
(19) Yeung, Ch.; Herrmann, K. A. *Macromolecules* **2003**, *36*, 229.
(20) Müller, M. *Macromolecules* **1997**, *30*, 6353.
(21) Yang, Y.; Char, K. *Macromol. Theory Simul.* **2001**, *10*, 565.
(22) John, A.; Nagel, J.; Heinrich, G. *Macromol. Theory Simul.* **2007**, *16*, 430.
(23) Cheng, M. H.; Balazs, A. C.; Yeung, Ch.; Ginzburg, V. V. *J. Chem. Phys.* **2003**, *118*, 9044.
(24) Berezkin, A. V.; Kudryavtsev, Y. V. *Macromolecules* **2011**, *44*, 112.
(25) Guseva, D. V.; Kudryavtsev, Y. V.; Berezkin, A. V. *J. Chem. Phys.* **2011**, *135*, 204904.
(26) Schulze, J. S.; Cernohous, J. J.; Hirao, A.; Lodge, T. P.; Macosko, C. W. *Macromolecules* **2000**, *33*, 1191.
(27) Schulze, J. S.; Moon, B.; Lodge, T. P.; Macosko, C. W. *Macromolecules* **2001**, *34*, 200.
(28) Jiao, J.; Kramer, E. J.; de Vos, S.; Möller, M.; Koning, C. *Macromolecules* **1999**, *32*, 6261.
(29) Oyama, H. T.; Ougizawa, T.; Inoue, T.; Weber, M.; Tamaru, K. *Macromolecules* **2001**, *34*, 7017.
(30) Jeon, H. K.; Macosko, C. W.; Moon, B.; Hoye, T. R.; Yin, Z. *Macromolecules* **2004**, *37*, 2563.
(31) Kim, H. Y.; Jeong, U.; Kim, J. K. *Macromolecules* **2003**, *36*, 1594.
(32) Yin, Z.; Koulic, C.; Pagnoulle, C.; Jérôme, R. *Langmuir* **2003**, *19*, 453.
(33) Zhang, J.; Lodge, T. P.; Macosko, C. W. *Macromolecules* **2005**, *38*, 6586.
(34) Yu, X.; Wu, Y.; Li, B.; Han, Y. *Polymer* **2005**, *46*, 3337.
(35) Kim, B. J.; Kang, H.; Char, K.; Katsov, K.; Fredrickson, G. H.; Kramer, E. J. *Macromolecules* **2005**, *38*, 6106.
(36) Harton, S. E.; Stevie, F. A.; Spontak, R. J.; Koga, T.; Rafailovich, M. H.; Sokolov, J. C.; Ade, H. *Polymer* **2005**, *46*, 10173.
(37) Kim, B. J.; Fredrickson, G. H.; Kramer, E. J. *Macromolecules* **2007**, *40*, 3686.
(38) Lamnavar, K.; Baudouin, A.; Maazouz, A. *Eur. Polym. J.* **2010**, *46*, 1604.
(39) Wang, D.; Fujinami, S.; Liu, H.; Nakajima, K.; Nishi, T. *Macromolecules* **2010**, *43*, 5521.
(40) Lyu, S. P.; Cernohous, J. J.; Bates, F. S.; Macosko, C. W. *Macromolecules* **1999**, *32*, 106.
(41) Bhadane, P. A.; Tsou, A. H.; Cheng, J.; Favis, B. D. *Macromolecules* **2008**, *41*, 7549.
(42) Macosko, C. W.; Guegan, P.; Khandpur, A. K. *Macromolecules* **1996**, *29*, 5590.
(43) Snedergaard, K.; Lyngaae-Jorgenson, J. *Polymer* **1996**, *37*, 509.
(44) Milner, S. T.; Xi, H. *J. Rheol.* **1996**, *40*, 663.
(45) Diaz, M. F.; Barbosa, S. E.; Capiati, N. J. *Polymer* **2002**, *43*, 4851.
(46) Freluche, M.; Iliopoulos, I.; Millequant, M.; Flat, J.-J.; Leibler, L. *Macromolecules* **2006**, *39*, 6905.
(47) Jiao, J.; Kramer, E. J.; de Vos, S.; Möller, M.; Koning, C. *Polymer* **1999**, *40*, 3585.
(48) Retsos, H.; Anastasiadis, S. H.; Pispas, S.; Mays, J. W.; Hadjichristidis, N. *Macromolecules* **2004**, *37*, 524.
(49) Jeon, H. K.; Zhang, J.; Macosko, C. W. *Polymer* **2005**, *37*, 12422.
(50) Hoogerbrugge, P. J.; Koelman, J. M. V. A. *Europhys. Lett.* **1992**, *19*, 155.
(51) Koelman, J. M. V. A.; Hoogerbrugge, P. J. *Europhys. Lett.* **1993**, *21*, 363.
(52) Espanol, P.; Warren, P. B. *Europhys. Lett.* **1995**, *30*, 191.
(53) Groot, R. D.; Warren, P. B. *J. Chem. Phys.* **1997**, *107*, 4423.
(54) Semenov, A. N. *Sov. Phys. JETP* **1985**, *61*, 733.
(55) Besold, G.; Vattulainen, I.; Karttunen, M.; Polson, J. M. *Phys. Rev. E* **2000**, *62*, R7611.
(56) Akkermans, R. L. C.; Toxvaerd, S.; Briels, W. J. *J. Chem. Phys.* **1998**, *109*, 2929.
(57) Khokhlov, A. R.; Berezkin, A. V.; Khalatur, P. G. *J. Polym. Sci. A., Polym. Chem.* **2004**, *42*, 5339.
(58) Liu, H.; Qian, H. J.; Zhao, Y.; Lu, Z. Y. *J. Chem. Phys.* **2007**, *127*, 144903.
(59) Gavrilov, A. A.; Guseva, D. V.; Kudryavtsev, Y. V.; Khalatur, P. G.; Chertovich, A. V. *Polym. Sci. Ser. A* **2011**, *53*, 1207.
(60) Berezkin, A. V.; Solov'ev, M. A.; Khalatur, P. G.; Khokhlov, A. R. *J. Chem. Phys.* **2004**, *121*, 6011.
(61) Helfand, E.; Tagami, Y. *J. Chem. Phys.* **1972**, *56*, 3592.
(62) Helfand, E.; Bhattacharjee, S. M.; Fredrickson, G. H. *J. Chem. Phys.* **1989**, *91*, 7200.
(63) Zhao, W.; Zhao, X.; Rafailovich, M. H.; Sokolov, J.; Composto, R. J.; Smith, S. D.; Russell, T. P.; Dozier, W. D.; Mansfield, T.; Satkowski, M. *Macromolecules* **1993**, *26*, 561.

(64) Welp, K. A.; Wool, R. P.; Agrawal, G.; Satija, S. K.; Pispas, S.; Mays, J. *Macromolecules* **1999**, *32*, 5127.
(65) Milner, S. T. *Macromolecules* **1994**, *27*, 2333.
(66) Berezkin, A. V.; Khalatur, P. G.; Khokhlov, A. R. *Macromolecules* **2006**, *39*, 8808.
(67) Groot, R. D.; Madden, T. G. *J. Chem. Phys.* **1998**, *108*, 8713.
(68) Ilnytskyi, J. M.; Patsahan, T.; Holovko, M.; Krouskop, P. E.; Makowski, M. P. *Macromolecules* **2008**, *41*, 9904.
(69) Lee, C.; Gido, S. P.; Poulos, Y.; Hadjichristidis, N.; Tan, N. B.; Trevino, S. F.; Mays, J. W. *Polymer* **1998**, *39*, 4631.
(70) Huang, Ch. I.; Yu, H. T. *Polymer* **2007**, *48*, 4537.
(71) Zhang, J.; Ji, S.; Song, J.; Lodge, T. P.; Macosko, C. W. *Macromolecules* **2010**, *43*, 7617.